

## COBRA-SFS Model and Results for NUHOMS-32PT Spent Fuel Storage Canister

### Description of COBRA-SFS Model

The NUHOMS-32PT spent fuel storage canister is modeled in COBRA-SFS using detailed subchannel noding for the fuel assemblies, and solid material nodes to represent the basket structure, support rails, and canister shell. The full axial length of the canister is included in the COBRA-SFS model using 44 axial nodes over the internal length of the canister, with upper and lower plenum models to represent heat transfer through the canister top and bottom. One-half section of symmetry of the canister is represented in the COBRA-SFS model, with the line of symmetry passing through the R45 support rails, as shown in Figure 1. Although the stainless steel basket itself is symmetrical on the vertical and horizontal axes as well as the diagonal axis used in the model, the L-shaped aluminum and neutron poison liner plates within the basket openings are not symmetrically arranged around all three axes. As a result, the basket structure can be treated as symmetrical for heat transfer only around the diagonal axis.<sup>1</sup>

The rod-and-subchannel noding within the 18 fuel assemblies comprising half the canister in the model represents each individual rod and subchannel of each assembly. This requires 225 rods and 256 subchannels for each full assembly, and 120 rods and 136 subchannels for each of the four assemblies cut in half by the line of symmetry. The model includes a total of 4,128 subchannels and 3,630 rods to represent the fuel assemblies. In addition, the open flow paths through the structure of the stainless steel support rails were modeled with isolated flow channels of appropriate dimensions, adding an additional 16 subchannels to the model. (The main reason for including these openings as flow channels was to permit calculation of radiative heat transfer between the elements of the rail structure. Because of the horizontal orientation of the canister, there is essentially no flow in these channels, and therefore no heat removal by natural convection.)

The canister shell, support rails, and basket assembly were modeled with 251 solid material nodes for the configuration with stainless steel support rails. With the solid aluminum support rails, the model included 252 solid material nodes. The solid material nodes in COBRA-SFS are used to represent conduction heat transfer through a structure as a network of thermal resistances. Nodes are defined by the geometric distance and cross-sectional area in the direction of heat flow, and the thermal conductivity of the material represented by the node. Nodes representing aluminum have the thermal properties of aluminum, nodes representing the neutron poison have the thermal properties of the neutron poison material, nodes representing stainless steel have the thermal properties of stainless steel, etc. Connections can be defined in any arbitrary orientation, to capture all connections between adjacent nodes, including connections to the flow channels within the assemblies.

Figure 2 illustrates the basket structure noding for a fuel assembly in the inner basket. Each L-shaped aluminum liner plate within the basket opening is represented with two nodes, one for each 'leg' of the plate (nodes 47 and 48 in Figure 2). The two nodes communicate with

---

<sup>1</sup> There is a slight asymmetry even on the diagonal axis, in that the liner plate geometries of two adjacent assemblies on the outer edge of the right side and bottom edge of the basket are transposed, but the effect should be negligible. The significant temperature gradients in the basket are in the radial direction, and not in the circumferential direction.

each other, and are also connected by appropriate thermal resistances to the fluid subchannels in the fuel assembly on one side, and the solid structure nodes of the L-shaped poison plate on the other side. Each poison plate is also represented with two nodes, one for each 'leg' of the L (nodes 49 and 50 in Figure 2). The nodes representing the poison plate connect to the immediately adjacent nodes modeling the stainless steel basket (nodes 51 and 53 in Figure 2). The stainless steel plates of the basket are represented with nodes on each of the four faces and at each of the four corners of the square lattice forming the opening for a single fuel assembly.

Two different designs for the basket support rail structures were submitted for the 32PT canister. In one design, the rails are constructed of stainless steel plates forming an open support lattice, with aluminum plates fastened to the inner surfaces of the steel in various locations. In the other design, the rails consist of solid aluminum castings with cross-sections that fit into the 'foot-print' of the stainless steel rails. These two designs are illustrated in Figure 3 (for the stainless steel rails) and in Figure 4 (for the solid aluminum rails). These two figures show only the R90 support rail; the R45 rails in each case are of the same configuration as the R90 rails, but are shaped to fit into the spaces formed by the 'corners' of the rectangular basket array within the canister shell. (Refer to Figure 1 for a view of the entire canister cross-section, showing R90 and R45 support rails for the solid aluminum configuration.)

Figure 3 illustrates the material nodes used in the COBRA-SFS model to represent the rail structures supporting the basket within the canister shell for the R90 rail of the stainless steel rail design. In this design, the support rails consist of steel plates that form an open, relatively hollow support structure. The figure shows the noding for the R90 stainless steel rail at the top of the canister. The rail nodes connect directly to the nodes representing the stainless steel basket, and perfect contact is assumed. Perfect contact is also assumed for the aluminum liner plates bolted to the stainless steel plates forming the support rail. Black body radiation view factors were specified for the surfaces of the flow channels formed by the openings within the stainless steel structure (enclosures 20 through 26 in Figure 3). Heat transfer due to radiative exchange between the aluminum plates and conduction through the backfill gas was calculated as part of the heat transfer solution for the system.

Figure 4 shows the material nodes used in the COBRA-SFS model to represent the R90 rail for the solid aluminum design. In this configuration, the flow channels and material nodes representing the steel and aluminum plates are replaced with solid material nodes representing the solid aluminum castings, per TN's drawings. The noding is relatively detailed, so that the model can represent any temperature gradients in the radial or circumferential directions in the rails. (These gradients are unlikely to be large in a solid aluminum structure, but if the nodes are not included in the model, the code cannot predict them.)

The canister shell was modeled with 21 solid material nodes, including 7 zero-thickness boundary nodes, used to impose selected surface temperature boundary conditions on the canister. A uniform gap of 0.08" was modeled for the thermal connections between the nodes representing the outer surface of the rails and the nodes modeling the canister shell. This connection was defined to include the effect of radiative heat transfer across the gap, as well as conduction through the fill gas.

Calculations were performed with COBRA-SFS for the two models described above, representing the NUHOMS-32PT canister with the stainless steel rail design, and with the solid

aluminum rail design. In addition, calculations were performed with a modified version of the model with solid aluminum support rails, in which the thermal conductivity of the basket material was specified with a value four times that of stainless steel. This was done to approximate in the COBRA-SFS modeling the effective thermal conductivity applied in the basket region in the TN analysis using the ANSYS code. These three modeling configurations were run for boundary conditions corresponding to normal long-term storage with helium in the canister, and for the vacuum case with uniform boundary temperature of 215 °F on the outer surface of the canister.

### Description of Transnuclear NUHOMS-32 PT ANSYS Model

The TN NUHOMS-32PT ANSYS model utilizes effective conductivities for heat transfer from the fuel assembly through the basket and associated components. Specifically, they apply effective conductivities for 1) the stainless steel plates comprising the basket and the assumed 0.0075” surrounding gas gaps (one on either side of each ligament, as assumed by TN) and 2) the L-shaped aluminum and neutron poison plates and the assumed 0.00375” gas gap (between the two plates) lining particular regions of the basket. These effective conductivities are defined using a parallel-path (along the layers) algorithm of the functional form,

$$k_{eff-along} = \frac{\sum_{n=1}^N k_n w_n}{\sum_{n=1}^N w_n} \quad (1)$$

where  $k_n$  = thermal conductivity of the  $n^{th}$  material included in the parallel path  
 $w_n$  = width of the  $n^{th}$  material normal to the direction of heat flow

Within the TN model, the effective conductivity is calculated using the above relationship for ANSYS material property definition numbers 1 and 6. When this effective conductivity is applied to heat transfer from the fuel assemblies in the NUHOMS-32PT canister, the parallel paths are treated as illustrated in Figure 5 and Figure 6.

Figure 5 represents the heat transfer path as modeled in ANSYS by TN for heat flow from the fuel assemblies through the “gas gap+XM-19+gas gap” sandwich that only exists in select locations. After passing through this incorrectly assumed parallel path to an XM-19 node, heat transfer along the XM-19 material heading out radially to the canister wall is treated as simply conduction through the XM-19 material. Coincidentally, only one gas gap should have been assumed given TN’s selected modeling approach. Figure 6 represents the heat transfer path as modeled in ANSYS by TN for heat flow from the fuel assemblies through the L-shaped “aluminum+gas gap+Poison plate” sandwich that only exists in select locations. After passing through this incorrectly assumed parallel path, the heat flows into the XM-19 stainless basket material through another incorrectly assumed parallel path as depicted in Figure 5, then radially outward to the canister wall.

This approach can be used to represent only the heat flow paths along the layers of the plates and the path along the axial length of the canister. It is not an appropriate representation of the heat flow path along the continuous XM-19 stainless steel plates to the support rails,

which is the primary route of heat removal. Axial heat transfer, which can be represented with the effective thermal conductivity based on parallel-paths, is capable of removing only a small part of the heat from the canister. As such, bi-directional material property definitions are required in order to accurately specify the orthotropic nature of heat conduction through these components, given TN's geometric construction approach.

The structure of the storage module in which the canister sits requires that the canister design allow the bulk of the heat to be removed through the sides of the canister. This means that most of the heat transfer is in the radial direction. Heat transfer in the radial direction from the fuel to the outer surface of the canister does not follow a parallel path (along the layers) from the fuel assemblies through the aluminum and neutron poison plates, gas gaps, and stainless steel basket structure. This is obvious from inspection of the cross-section of the canister internals shown in Figure 1. On two of the sides of the basket enclosure for any given fuel assembly, the rods will see only the stainless steel plates, and on these faces, heat transfer is directly from the fuel assembly to the basket, by radiation to the stainless steel and conduction *through* the gas gap surrounding the fuel assembly. (Convection can also occur in the fill gas, but in the horizontal configuration, it plays an insignificant role.) On the two other sides, the fuel rods see the aluminum liner plates. Heat transfer on these faces therefore must follow a serial path (*through* the layers), first to the aluminum liner plate, then across the small gas gap between the Al and neutron poison plates, then through the poison plate and across the next gas gap into the stainless steel basket.

Shown in Figure 7 is a conceptual representation of these "radial" heat transfer paths through the basket. In no case can the heat flow be treated as following a parallel path (along the layers) exclusively, as described by Eq. (1) above. The effect of using a  $k_{eff-along}$  defined as in Eq. (1) for heat transfer "through" the basket cell edges, gaps and ancillary components results in a significant overestimation of the effective thermal conductivity of the basket structure. Using the path featured in Figure 5 as an example, in this case for the direction passing through the left or upper wall of the "cell" depicted in Figure 3 involving helium, the applied effective thermal conductivity ( $k_{eff-along 1}$ ) works out to be a little more than four times that which should have been applied ( $k_{eff-through 1}$ ) as illustrated by the following calculations.

$$k_{eff-along 1} = \frac{k_{XM-19} w_{XM-19} + 2 \cdot k_g w_g}{2 \cdot w_g + w_{XM-19}}$$

and

$$k_{eff-through 1} = \frac{w_{XM-19} + 2 \cdot w_g}{\frac{w_{XM-19}}{k_{XM-19}} + \frac{2 \cdot w_g}{k_g}}$$

where  $k_{XM-19}$  = thermal conductivity of XM-19  
 $w_{XM-19}$  = width of the XM-19 plate  
 $k_g$  = thermal conductivity of fill gas  
 $w_g$  = width of gas gap assumed on both sides of basket plates

Inserting appropriate values for these thermal conductivities and using the specified dimensions of the various components yields a value for  $k_{eff\text{-}along\ 1}$  that works out to be approximately 4.3 to 4.7 times larger than  $k_{eff\text{-}through\ 1}$ .

$$k_{eff\text{-}along\ 1} \cong 4.5 \cdot k_{eff\text{-}through\ 1}$$

Making an example of the path featured in Figure 6, for the direction passing through the right or lower wall of the “cell” depicted in Figure 7, the applied effective thermal conductivity ( $k_{eff\text{-}along\ 2}$ ), for the Al/neutron poison materials sandwiching the assumed 0.00375” gas gap (excluding the XM-19 and surrounding gap gas), works out to be around thirty times that which should have been applied ( $k_{eff\text{-}through\ 2}$ ), as illustrated by the following calculations.

$$k_{eff\text{-}along\ 2} = \frac{k_{Al} w_{Al} + k_g w_g + k_{NP} w_{NP}}{w_{Al} + w_g + w_{NP}}$$

and

$$k_{eff\text{-}through\ 2} = \frac{w_{Al} + w_g + w_{NP}}{\frac{w_{Al}}{k_{Al}} + \frac{w_g}{k_g} + \frac{w_{NP}}{k_{NP}}}$$

where  $k_{Al}$  = thermal conductivity of aluminum  
 $w_{Al}$  = width of the aluminum plate  
 $k_g$  = thermal conductivity of fill gas  
 $w_g$  = width of gas gap assumed between plates  
 $k_{NP}$  = thermal conductivity of neutron poison plate  
 $w_{NP}$  = width of the neutron poison plate

Values of  $k_{eff\text{-}along\ 1}$  and  $k_{eff\text{-}along\ 2}$  were applied in all directions in the ANSYS model supplied by TN, to define the effective thermal conductivity in the bodies representing 1) the basket material region and 2) the Al/neutron poison plate region. These material regions were not modeled in ANSYS with separate material orientation (orthotropic) and property definitions. Hence, the same values of  $k_{eff\text{-}along\ 1}$  and  $k_{eff\text{-}along\ 2}$  were applied in both the “along” and “through” directions.

It could be argued that this lumping of material properties is an appropriate representation for heat transfer through the basket material in the *axial* direction (from canister end to end), but it is obviously not correct in the radial direction involving “through” heat paths. Heat transfer must pass serially through the aluminum and neutron plates and associated gas gaps and then into and through the XM-19 stainless steel basket structure to travel out to the support rails.

The conceptual error of the modeling approach used by TN to represent radial heat transfer through the basket region of the canister is similar to the error uncovered earlier in TN’s approach to representing the material properties of the stainless steel support rails in the extremities of the canister. In that case, the stainless steel and aluminum components of the rails were represented as a single homogeneous material, using an effective conductivity that was supposed to represent perfect parallel heat transfer paths through the stainless steel and the aluminum. As with the case of the basket region components, however, the heat transfer paths

are parallel only in the axial direction. In the radial direction, the SST/Al rails have no continuous path for conduction through the aluminum. Virtually all of the heat flowing radially must go through the stainless steel alone. (It should be noted, however, that there is a minor parallel path via radiation between the aluminum plates within the open structure of the stainless steel rails, but at the temperatures within the rails, this can provide only a minor contribution to the total heat transfer, and will be only a small fraction of the conduction heat transfer rate at the same temperatures. Besides, the documentation of the TN model notes that radiative heat transfer in this region was neglected, as a measure of conservatism in the analysis.)

### **Comparison of Transnuclear ANSYS model and COBRA-SFS Model of NUHOMS-32 PT**

Figure 8 shows a comparison of the ANSYS and COBRA-SFS results for the NUHOMS-32PT canister in vacuum with stainless steel rails and a uniform boundary condition of 215 °F imposed on the canister surface. Figure 9 shows a similar comparison for the NUHOMS-32PT canister in vacuum with solid aluminum rails. Both of these figures include a diagram of the canister cross-section showing the lines along which the plotted temperature profiles were obtained. The temperature profiles representing the ANSYS results were taken along a vertical line passing through the centers of the fuel assemblies just to the right of the canister geometric centerline. (The gap between the rail inner plate adjacent to the basket and the outer curved rail plate next to the canister shell is reflected in the two large gaps in the otherwise solid line representing the ANSYS temperature profile.) For the COBRA-SFS results, the profile for the fuel temperatures follows a vertical line passing through the centers of the fuel assemblies just to the right of the canister geometric centerline. The temperature profile through the basket follows the geometric centerline of the canister, showing the predicted temperatures along the center stainless steel plate of the basket to the rails, then through the center of the R90 rail at the top of the canister, and through the canister shell. In all cases, the profiles were taken at the axial location of the peak fuel temperature.

The profiles in Figure 8 show that the ANSYS and COBRA-SFS models predict essentially the same thermal behavior in the fuel assemblies when the canister is in vacuum. Figure 8 also shows that the temperatures predicted with the ANSYS model in the stainless steel rails are significantly different from the COBRA-SFS results. In the ANSYS profile, the temperature difference between the inner plate of the rail and the outer curved plate of the rail is unrealistically small for the physical conditions (only about 30 °F). The temperature difference between the outer rail plate and the inner surface of the canister shell is unreasonably large (approximately 340 °F over a distance of 0.08"). By contrast, the COBRA-SFS results predict a temperature drop of approximately 145 °F across the structure of the stainless steel rails, and a temperature drop of only about 135 °F across the assumed gap between the outer edge of the rails and the canister shell.

The temperature profile in the rail region predicted with the ANSYS model results from the inappropriate superposition of heat conduction through the stainless steel structure of the rails and the aluminum plates fastened to the inner surfaces of the steel plates forming the rails. In the ANSYS model, these conductivities are treated as parallel heat transfer paths through the structure of the rails, when in fact there is no parallel path from the basket to the outer edge of the rail through the aluminum plates. The only available continuous conduction path is through the stainless steel. The only heat transfer benefit that can be conferred by the aluminum plates is to enhance radiative heat transfer across the open lattice of the rail structure. However, this

mode of heat transfer was neglected (as a conservatism) in the ANSYS analysis, as stated by TN. (It was included in the COBRA-SFS model, however.) The aluminum plates will also help flatten the temperature profile in segments of the stainless steel plates of the rails to which they are directly attached, in effect creating some local and relatively short parallel paths. Because the aluminum plates are discontinuous, however, there is no parallel path for heat flow all the way through the rail. All heat must flow through stainless steel only at many points, and an electrical network analogy for heat flow in the rail structure would be an essentially serial path through the thermal resistance of the stainless steel.

The profiles in Figure 9, comparing the ANSYS and COBRA-SFS results for vacuum conditions with the solid aluminum rails, further illustrate this problem. When the appropriate thermal conductivities are used in the basket and rail regions, as shown by the COBRA-SFS results, the peak clad temperature is 801 °F, more than 112 °F above the value of 713 °F predicted with the ANSYS model. COBRA-SFS results obtained with the thermal conductivity of the basket artificially enhanced to about four times that of stainless steel lower the predicted peak clad temperature to about 647 °F; approximately 155 °F lower than the peak temperature predicted for the same design with the thermal conductivity of the solid nodes of the basket modeled correctly. This result is lower than the ANSYS results by about 65 °F, mainly because the COBRA-SFS model does not include most of the conservative assumptions incorporated in the ANSYS model. (In general, COBRA-SFS is applied using 'best estimate' modeling assumptions, and will usually predict temperatures somewhat lower than conservative licensing calculations.) In this case, these results show how sensitive the peak clad temperature is to thermal properties of the basket material. When the canister is in vacuum, the dominant mode of heat transfer from the fuel to the basket is radiation, and heat moves through the basket to the rails almost exclusively by conduction through the stainless steel plates of the basket.

The profiles in Figures 10 and 11 show comparisons of ANSYS and COBRA-SFS predictions of temperature profiles for both the stainless steel and solid aluminum rail designs with helium as the fill medium rather than vacuum. These profiles show essentially the same thermal behavior and temperature trends as were noted for the vacuum case. The only significant difference is that the peak temperatures are somewhat lower, due to the relatively high thermal conductivity of helium in comparison to the thermal conductivity of the extremely attenuated air in the vacuum case.

Another discrepancy noted in the TN ANSYS model was the large difference in the peak clad temperatures predicted for the helium and vacuum cases for the stainless steel rail design. In the ANSYS calculations, the peak clad temperature for the vacuum case is 875 °F, and for the helium case it is only 613 °F; a difference of about 262 °F, in contrast to the difference of approximately 130 °F obtained in the COBRA-SFS calculations. This result is contrary to experimental data obtained in instrumented spent fuel canisters for a wide range of decay heat loads, geometric designs, and storage orientations, with backfill media that included air, helium, and vacuum storage. The increased effective thermal conductivity in the basket region (and in the rails, for the stainless steel rail design) results in a significant under prediction of the peak clad temperature in the ANSYS calculations. The results obtained in the TN ANSYS model do not appear to agree with published data.

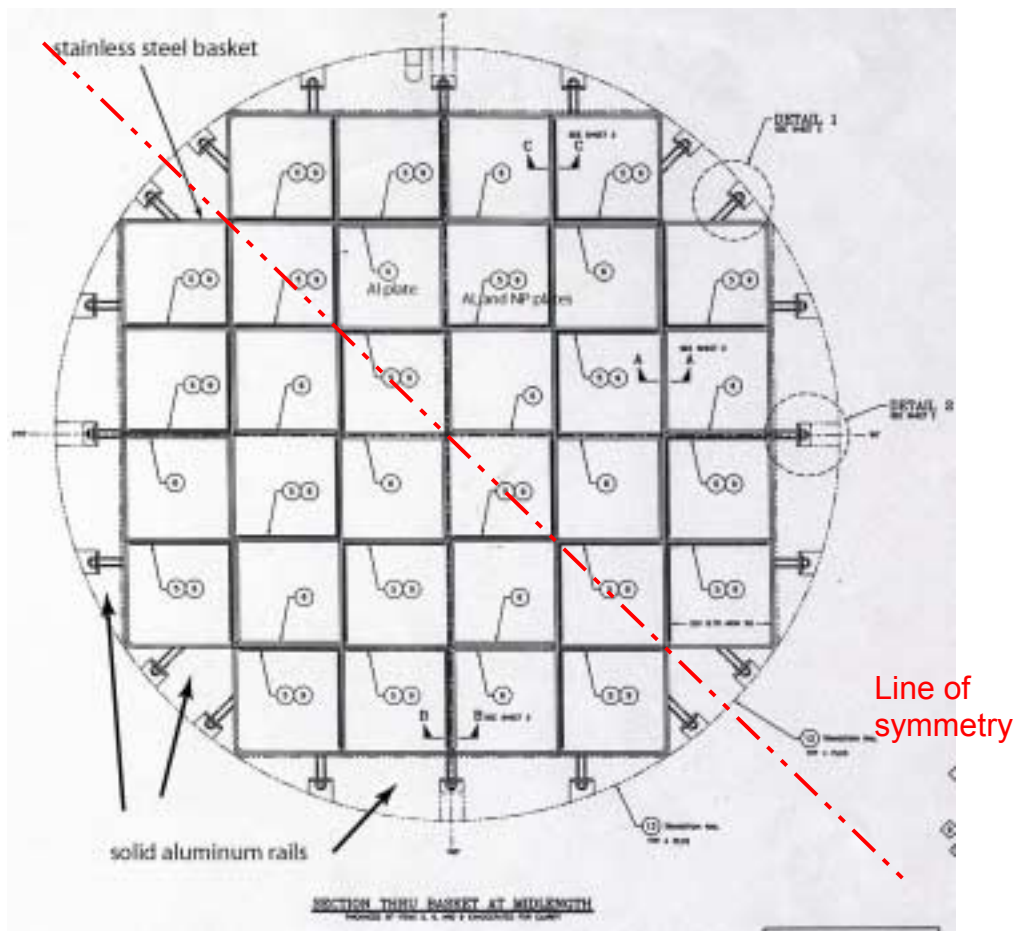


Figure 1. Cross-section of NUHOMS-32PT canister model showing radial symmetry of basket structure

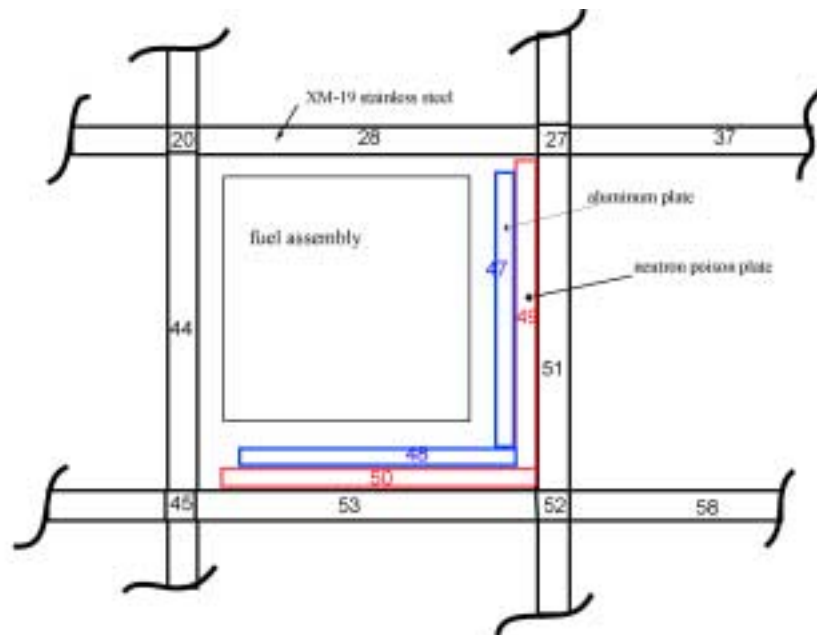


Figure 2. Illustration of solid conduction nodes in COBRA-SFS model representing stainless steel basket and liner plates comprising NUHOMS-32PT storage canister internals

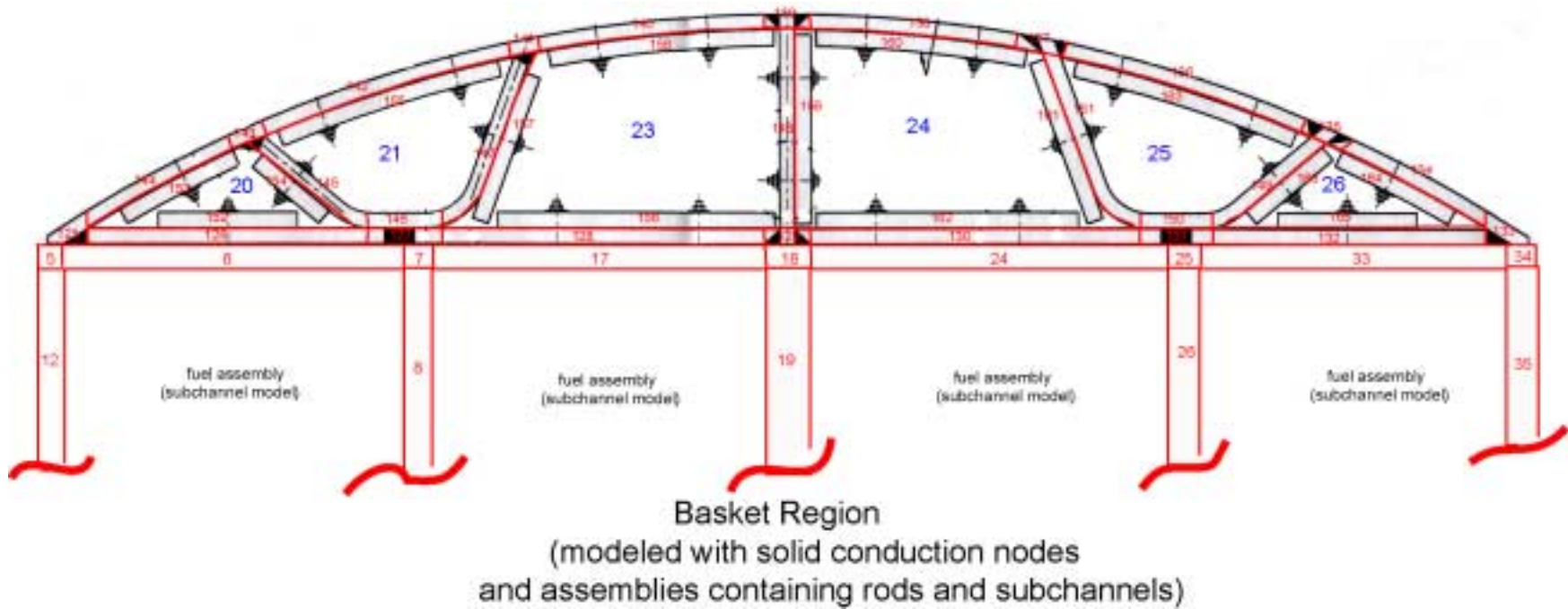


Figure 3. Illustration of solid conduction nodes in COBRA-SFS model representing the open structure R90 stainless steel rails with aluminum liner plates for NUHOMS-32PT storage canister internals

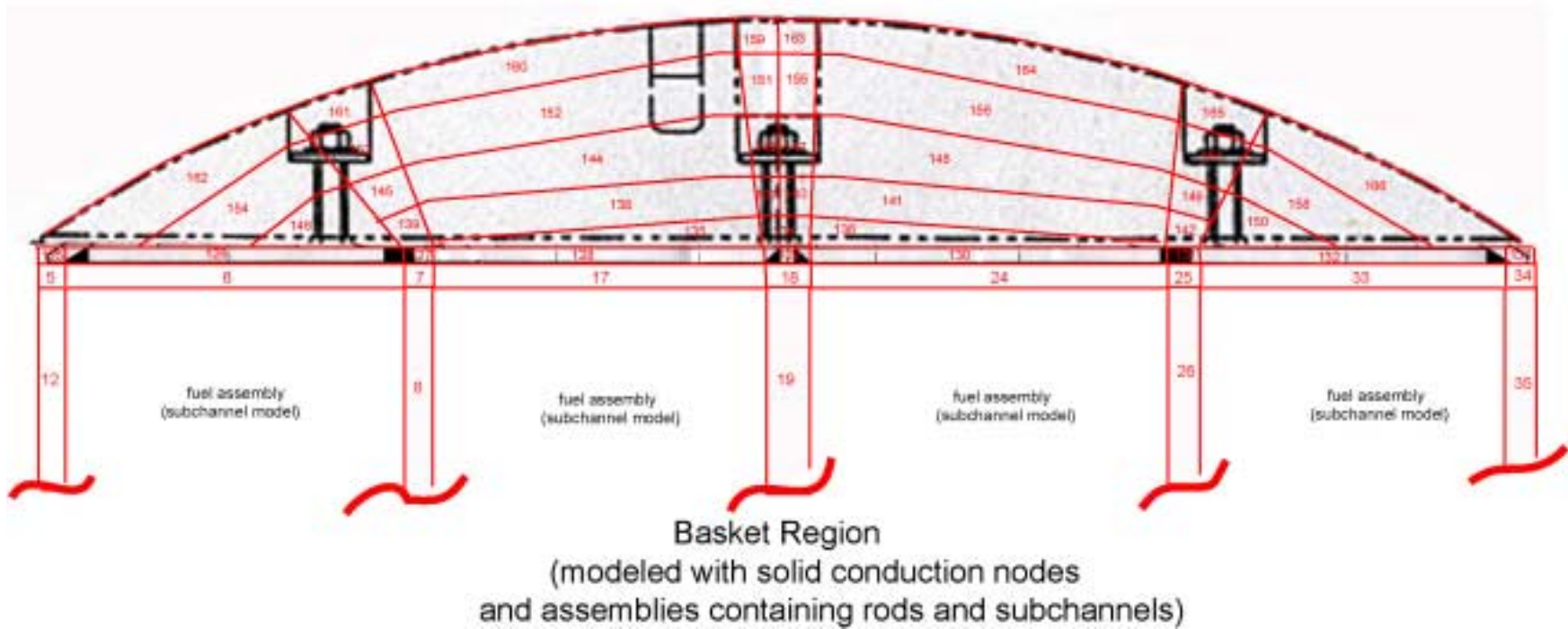


Figure 4. Illustration of solid conduction nodes in COBRA-SFS model representing the R90 solid aluminum rails for NUHOMS-32PT storage canister internals

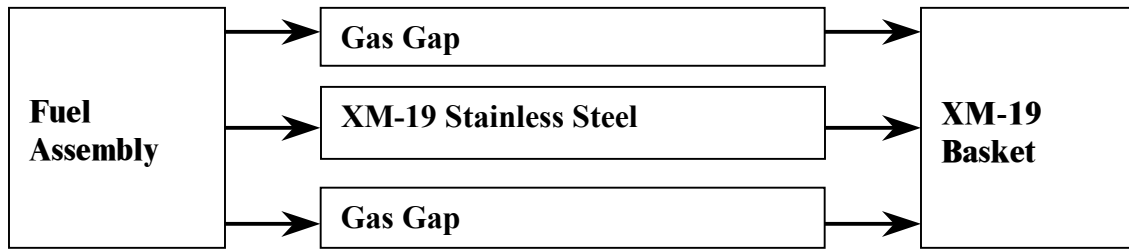


Figure 5. Illustration of parallel path  $k_{eff-along 1}$  assumed in TN's ANSYS model for the XM-19 basket plate and assumed 0.0075" gas gap on either side

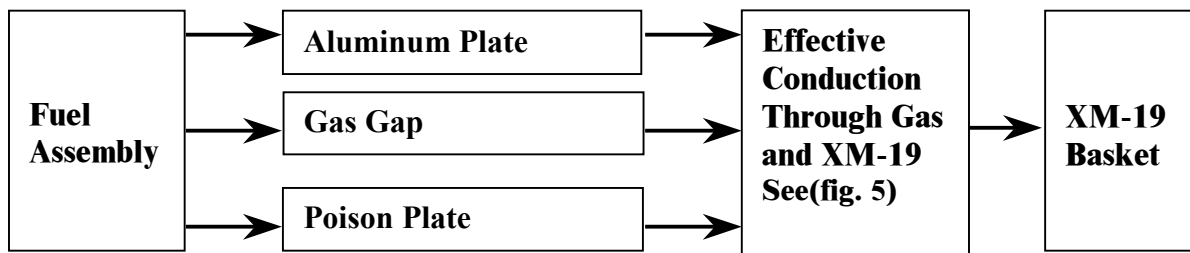


Figure 6. Illustration of parallel path  $k_{eff-along 2}$  assumed in TN's ANSYS model for the L-shaped aluminum and neutron poison plates and the associated 0.00375" gas gap

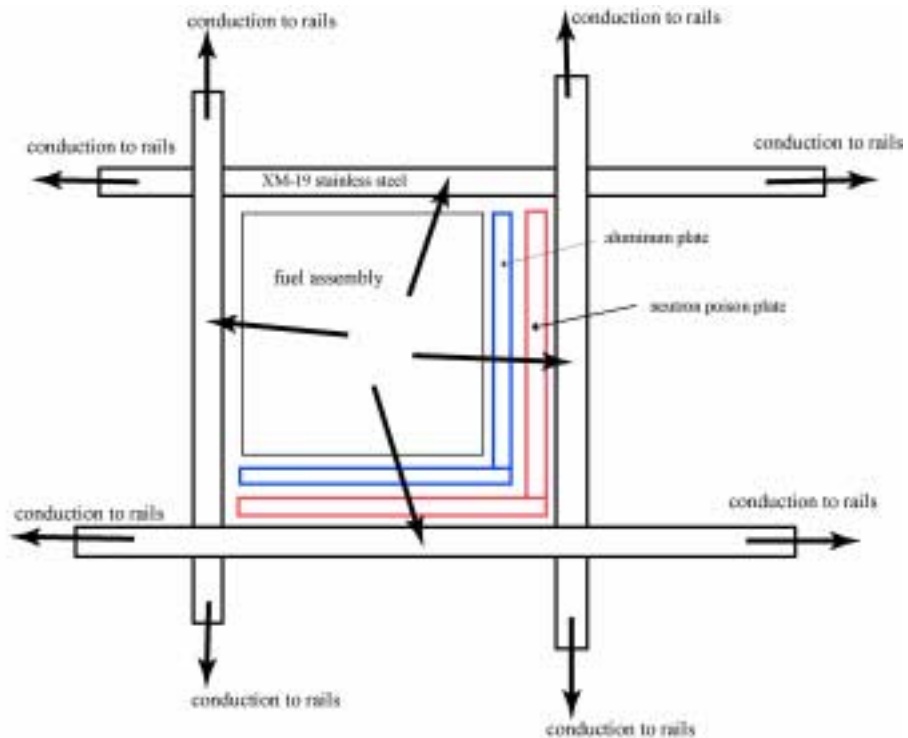


Figure 7. Conceptual diagram of radial heat flow through the basket region

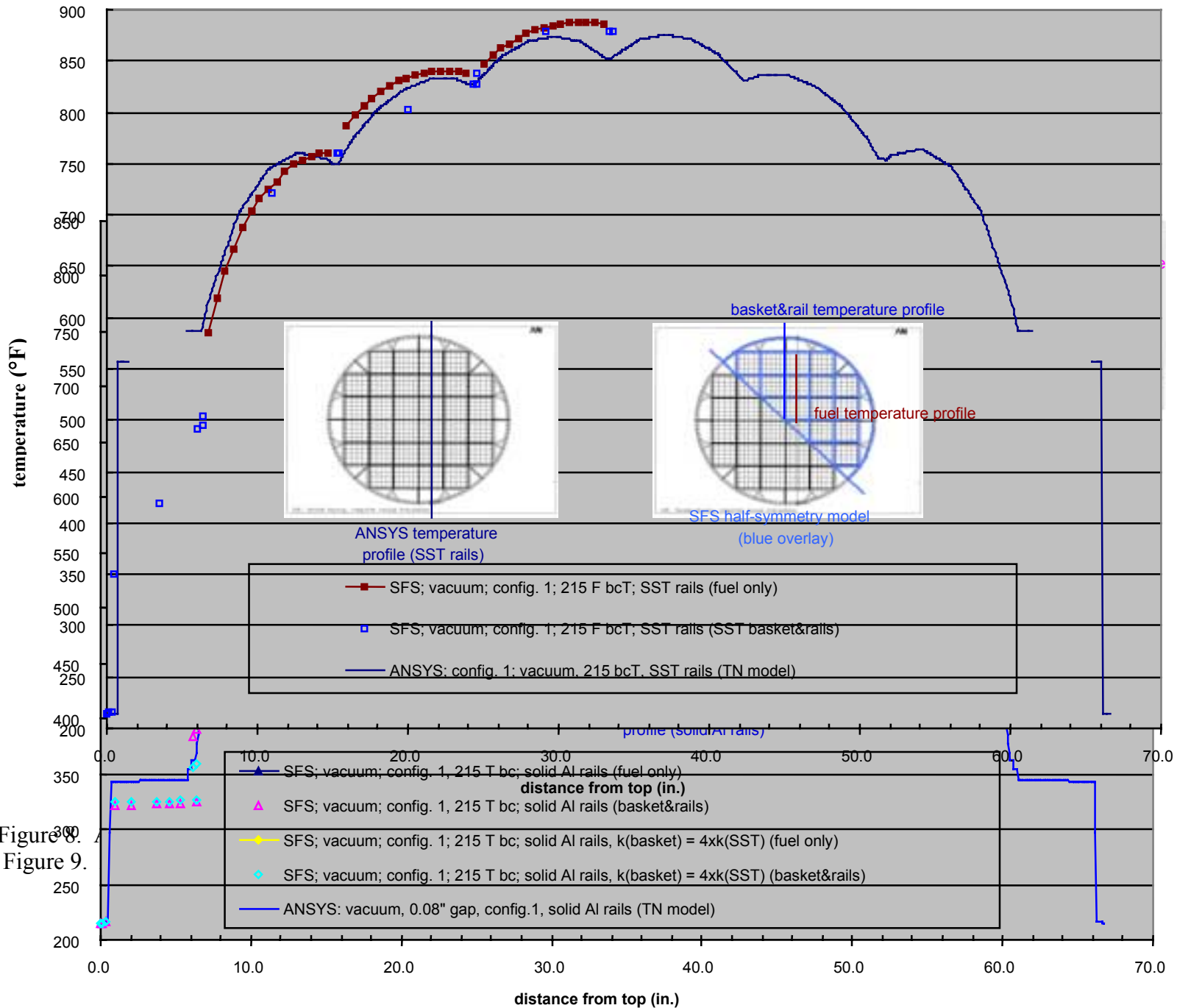


Figure 8.  
Figure 9.

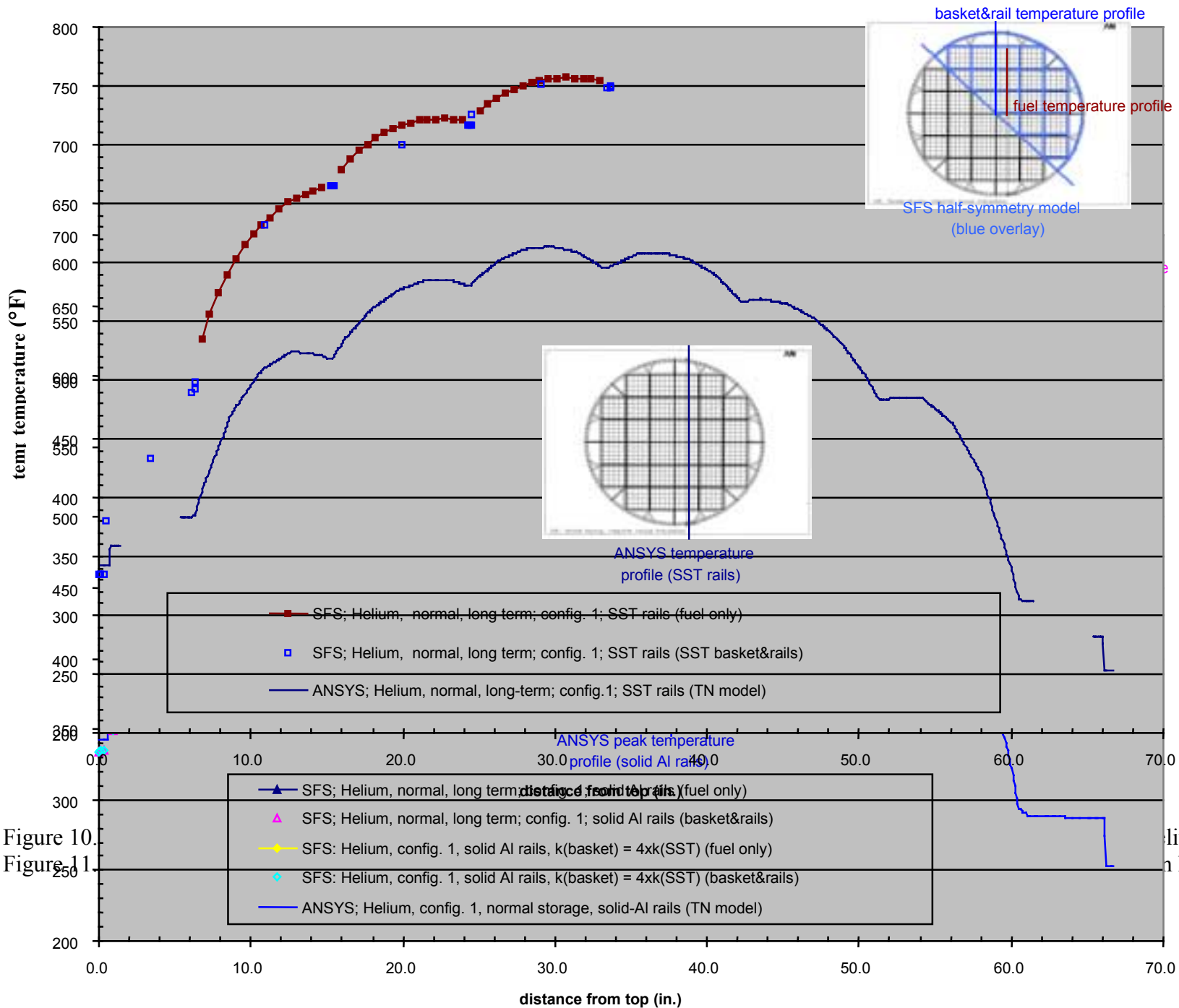


Figure 10.  
Figure 11

Helium  
in helium